Supplementary Materials for

Restoring Voluntary Control of Locomotion after Paralyzing Spinal Cord Injury

Rubia van den Brand, Janine Heutschi, Quentin Barraud, Jack DiGiovanna, Kay Bartholdi, Michèle Huerlimann, Lucia Friedli, Isabel Vollenweider, Eduardo Martin Moraud, Simone Duis, Nadia Dominici, Silvestro Micera, Pavel Musienko, Grégoire Courtine*

*To whom correspondence should be addressed. E-mail: gregoire.courtine@epfl.ch

Published 1 June 2012, *Science* **336**, 1182 (2012)
DOI: 10.1126/science.1217416

This PDF file includes:

Other Supplementary Material for this manuscript includes the following:
(available at www.sciencemag.org/cgi/content/full/336/6085/1182/DC1)

Supporting Online Material

Materials and Methods

Animals and behavioral training

Experiments were conducted on adult female Lewis rats (200-220 g body weight) housed individually on a 12-hour light/dark cycle with access to food and water *ad libitum*. All experimental procedures were approved by the Veterinary Office of the Canton of Zurich. Prior to surgery, all the rats (non-trained and trained) were first acclimatized to wearing the custom-made jacket for 1-2 weeks while navigating freely along the runway. The rats were then trained for an additional 1-2 weeks to walk bipedally. All the rats learned this task rapidly. Typically, they produced consistent stepping patterns within 1-2 sessions (**fig. S5**). Positive reinforcement (food reward) was used to encourage the rats to perform the requested tasks.

Surgical procedures

All basic surgical procedures and post-operative care for SCI rats have been described in detail previously (*6, 8, 10*). Briefly, under general anesthesia and aseptic conditions, bipolar EMG electrodes were inserted into hindlimb muscles. Two stimulating electrodes were secured onto the dura at the midline of spinal levels L2 and S1. After pre-lesion recordings, rats received a left T7 lateral over-hemisection and a right lateral hemisection at T10 (*8*). For the T7 over-hemisection, we aimed at interrupting the dorsal column bilaterally while sparing ventral pathways on the contralateral side (**fig. S1**). The completeness of the hemisections was assessed on 30-µm thick longitudinal sections incubated in serum containing anti-GFAP (1:1000, Dako, USA) antibodies. In addition, we confirmed the absence of BDA-labeled corticospinal axons in the dorsal column of the T8 spinal segment in transverse sections.

Multi-system neuroprosthetic training

Ten min prior to training, the rats received a systemic (I.P.) administration of quipazine (5-HT2A/C, 0.2 - 0.3 mg/kg), SKF-82197 (D1, 0.1 - 0.2 mg/kg) and 8-OH-DPAT (5-HT1A/7, 0.05 - 0.2 mg/kg). During training, we delivered monopolar electrical stimulation (0.2ms, 100-300µA, 40Hz) through L2 and S1 electrodes. Locomotor training was conducted bipedally on a treadmill (9 cm/s) with vertical robotic support, as well as overground with a robotic postural interface (**fig. S3**). The content of each training session evolved with the actual capacities of the rats and training objectives, as detailed in **fig. S3**. Positive reinforcement was used to encourage the rats to perform the requested tasks. An additional group of rats was trained with the same frequency and duration, but rehabilitation was restricted to step training on a treadmill. These rats were trained to walk bipedally overground with the robotic postural interface for 2 weeks prior to the lesion. They were also tested in this paradigm at 1 and 9 weeks post-lesion. At the end of the training period, treadmill-trained rats practiced overground locomotion with the robotic postural interface for about 10 min per day during 4-8 sessions to ensure that the specificity of the task was not responsible for their incapacity to initiate and sustain locomotion.

Kinematic, kinetic and EMG recordings and analysis

Bipedal locomotion was recorded on a treadmill (9 cm/s) as well as overground. The different paradigms and their features can be found in **fig. S2**. Kinematic (12 cameras, 200 Hz), kinetic (force plate, 2 kHz) and EMG (2 kHz, 10–1000 Hz bandpass) recordings were performed using

an integrated motion capture system. Procedures for data collection, data analysis, and computation have been described in detail previously (*6, 10*). The complete list of computed gait, kinematic, kinetic and EMG variables is reported in **Table S1**. To quantify locomotor performance, we applied a principal component (PC) analysis on all the computed variables (*10*). **Fig. S5** provides a step-by-step explanation of the procedure and interpretation. We quantified recovery of locomotor function as the distance between gait cycles of intact and injured rats in the 3D space created by PC1-3 (*29*).

Brain stimulation and recordings

A monopolar electrode was implanted epidurally over the left hindlimb motor cortex. A train of stimuli (0.2ms, 10ms pulse length, 300 Hz, 0.5 -1.5 mA) was delivered during bipedal standing in fully awake conditions. Testing was performed without and with electrochemical stimulations. Peak-to-peak amplitude and latency of evoked responses were computed from EMG recordings of the left TA muscle.

Neuronal modulations

At 60-70 days post-injury, a microwire array (16 or 32 channel) was implanted stereotaxically into layer V of the hindlimb area of the left motor cortex (**Fig. 4**). Recordings were conducted 5-7 days post-surgery. Neural signals were acquired (24.4 kHz) with a neurophysiology workstation synchronized to kinematic recordings. All spike-sorting was performed offline via super-paramagnetic clustering (*30*). Clusters were manually tuned based on established principles (*31*) to identify single units. Modulations were analyzed in single experimental sessions to avoid potential instability confounds. Two recurring behaviors were used to evaluate the significance of neuronal modulations. (i) *Initiation* was defined as swing onset from rest. (ii) *Correction* was defined as beginning of swing phase after irregular gait (**fig. S14**). A two-sample Kolmogorov-Smirnov test compared firing rates (estimated in 250ms windows) in successive, one-second periods encompassing initiation and correction to determine whether modulations were significant.

NMDA and Muscimol microinjections

To ablate T8-T9 neurons, we infused NMDA (1% in dH_2O) into 14 sites (depth 1 mm, total volume 3 µl) covering spinal levels T8-T9. Rats were tested 5 days post-lesion, and sacrificed on the following day. The ablation of neurons was verified *post mortem* on tissue sections stained with mouse anti-NeuN (1:500, Chemicon, USA) antibodies. To inactivate the motor cortex, we injected the GABA-agonist muscimol intra-cortically (800nl, 4.5 mg/Kg). Five days prior to experiments, we stereotaxically implanted a catheter (OD: 0.61 mm, ID: 0.28 mm) into the left motor cortex at a depth of 1.5 mm (**Fig. 4D**). Proper catheter location was verified *post mortem* on tissue sections stained for fluorescent Nissl visualization (Invitrogen, USA).

Tracing and immunohistochemistry

We conducted retrograde tract tracing by infusing Fastblue (2% in 0.1M phosphate buffer and 2% dimethyl sulfoxide) bilaterally into L1-L2 spinal segments (*8*). A total of 1.2 µl was pressure-injected over 6 sites (depth 1.5 mm). To trace motor cortex axonal projections, we injected the anterograde tracer BDA 10,000 (10% in 0.01M PBS) into the left motor cortex over 6 sites covering the hindlimb area (coordinates centered -1 mm rostrocaudal and -1.75 mm mediolateral to Bregma, depth 1.5 mm). The rats were perfused 18 days later with Ringer's solution containing 100 000 IU/L heparin and 0.25% $NaNO_2$ followed by 4% phosphate buffered paraformaldehyde, pH 7.4 containing 5% sucrose. For cfos experiments, rats were perfused 60

min after cessation of a 45 min bout of continuous locomotion (*6*). Locomotion was performed overground for intact and overground-trained rats, and during overground guided locomotion for treadmill-trained and non-trained rats in order to ensure the presence of stepping in all the animals. The brain, brainstem, and spinal cords were dissected, post-fixed overnight, and transferred to 30% phosphate buffered sucrose for cryoprotection. After 4 days, the tissue was embedded and sectioned on a cryostat at a 40-µm thickness.

For immunohistochemistry experiments, sections were incubated in serum containing rabbit anti-cfos (1:2000, Santa Cruz Biotechnologies, USA), anti-GFAP (1:1000, Dako, USA), or anti-5HT (1:5000, Sigma Aldrich, Germany), or mouse anti-synaptophysin (1:1000, Millipore, USA) antibodies. Immunoreactions were visualized with secondary antibodies labeled with Alexa fluor® 488 or 555. BDA-labeled fibers were detected using streptavidin-horseradish peroxidase (1:200) in 0.1M PBS-Triton (1%). Tyramide signal amplification Cyanine 3 was used at a dilution of 1:100 for 1 min.

Neuromorphological evaluations

Fastblue- and cfos-positive neurons were counted using image analysis software on 5 evenly spaced slices separated by 1.2 mm and centered on the T8-T9 junction. Fiber density was measured using 5 confocal image stacks per region per rat acquired with standard imaging settings and analyzed using custom-written scripts according to previously described methods (*32*). Confocal output images were divided into square regions of interest (ROI), and densities computed within each ROI as the ratio of traced fibers (amount of pixels) per ROI area. Files were color-filtered and binarized by means of an intensity threshold. Threshold values were set empirically and maintained across sections, animals and groups. Comparisons of computerized and manual counting of CST labeling in T8-T9 showed no differences between both methods. Manual fiber counts were conducted on spinal cord sections overlaid with 5 vertical lines. Fibers crossing these lines within the grey matter were marked, and all intersecting fibers on 3 sections per rat were summed to obtain a cumulative count. Both manual and computerized counts were performed blindly. Image acquisition was performed using a laser confocal scanning microscope and the LAS AF interface and stacks were processed offline.

Statistics

All data are reported as mean values ± s.e.m. Statistical evaluations were performed using one- or two-way ANOVA, repeated-measures ANOVA, or non-parametric Wilcoxon tests. The *post hoc* Kruskall-Wallis test was applied when appropriate.

Author Contributions

R.B. and J.H. made critical primary contributions to this study. P.M., J.H., L.F., J.D. and G.C. performed the surgeries. R.B., M.H., L.F., S.D., I.V. and N.D. trained the rats, and performed and analyzed the functional/behavioral experiments. J.H., Q.B., K.B. and E.M.M. performed and analyzed the anatomical experiments. J.D., R.B., and S.M. performed and analyzed the electrophysiological experiments. J.H. and G.C. prepared the figures with the contribution of all the authors. G.C. wrote the manuscript and all the authors contributed to its editing. G.C. conceived and supervised all aspects of the work.

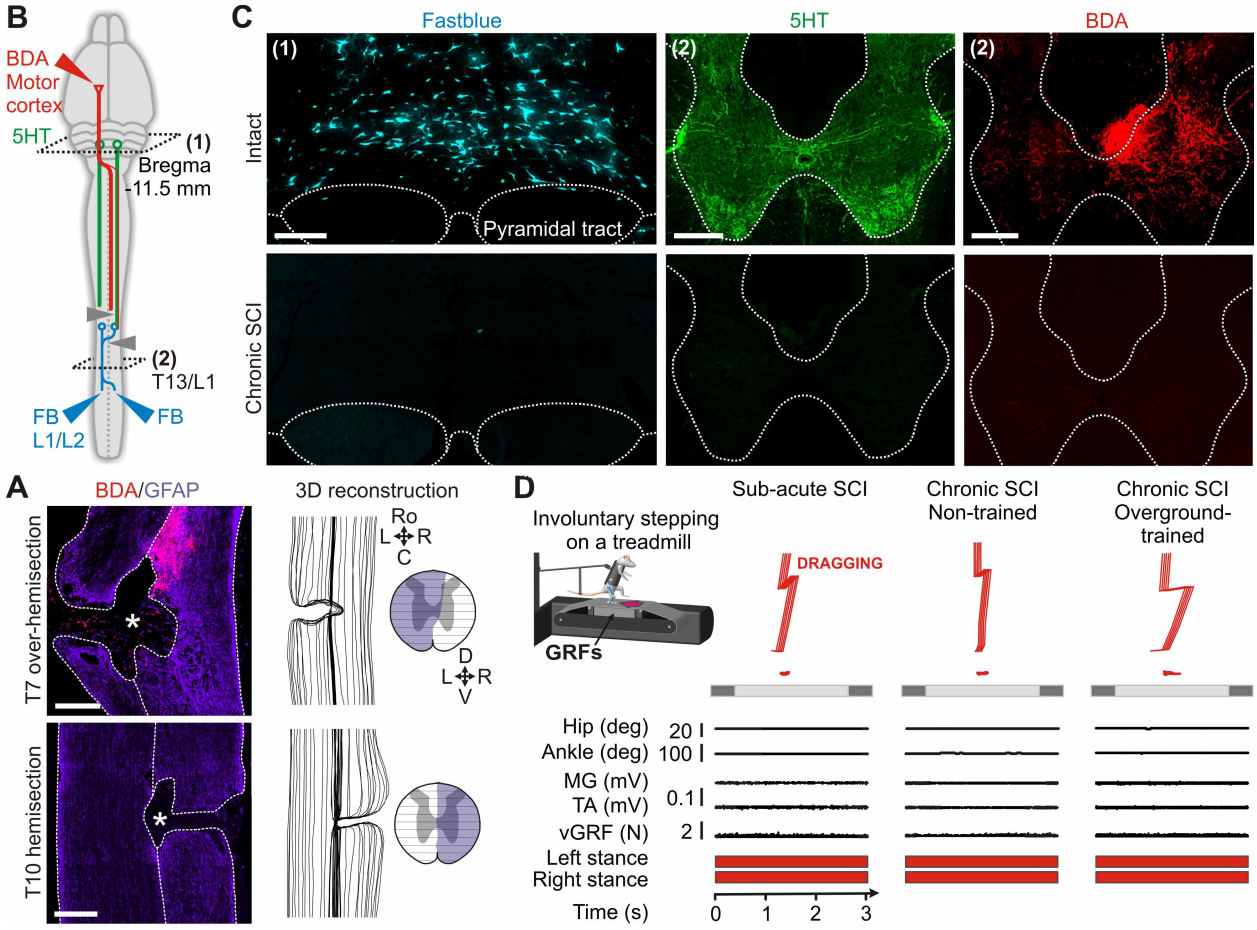

Fig. S1 | Staggered lateral hemisections induce a complete interruption of direct supraspinal pathways, leading to a complete and permanent paralysis of both hindlimbs. (A) Epifluorescent images as well as longitudinal and coronal views of a 3D reconstruction of the T7 lateral over-hemisection and T10 lateral hemisection. Scale bar, 500µm. We placed an over-hemisection at T7 in order to interrupt all the corticospinal fibers running in the dorsal column, thus only sparing the few (1-2%) fibers running through the right dorsolateral funiculus. **(B)**. Diagram illustrating anatomical experiments. **(C)** Combinations of retrograde (Fastblue, FB) and anterograde (biotinylated dextran amine, BDA) tracers together with immunolabeling of 5HT fibers show the complete and permanent absence of direct connections between spinal locomotor circuits and supraspinal centers. Scale bar, 300µm. **(D)** Rats were positioned in a bipedal posture above a moving treadmill belt (9 cm/s) while secured in a jacket that was attached to a robotic arm. Recordings at 1 and 9 weeks post-injury without electrochemical stimulations, both in non-trained and overground-trained rats, showed the complete and permanent absence of spontaneous hindlimb locomotor movements and vertical ground reaction forces (vGRF), as well as the quiescent EMG activity of tibialis anterior (TA) and medial gastrocnemius (MG) muscles.

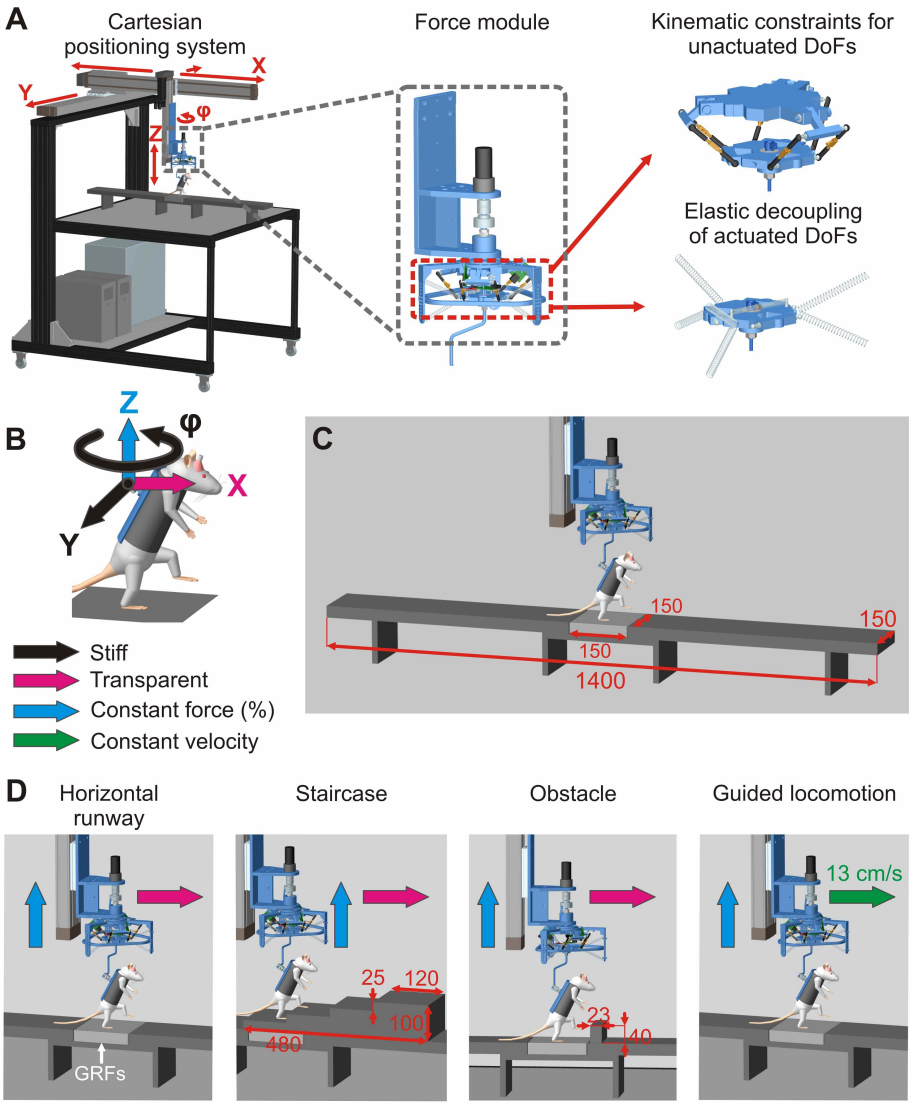

Fig. S2 | Robotic postural interface to enable bipedal locomotion across a variety of paradigms. (A) The robot consists of an actuated Cartesian positioning system that allows translations of the rat in the horizontal plane (X, Y) while providing vertical support (Z). An additional motor at the end-effector of this serial structure actuates rotation (φ). This serial configuration provides a large workspace in which forces can be applied to the rat in 4 degrees of freedom (DoFs). To hide the inertia of the massive positioning robot, we developed a novel force module based on a series elastic actuator (SEA). A SEA is composed of an actuator that is complemented with a passive compliant element in series. This compliant interface effectively decouples the actuator's inertia to achieve a transparent supporting system; the rat does not "feel" the presence of the robot. **(B)** The rat is positioned in a custom-made, skin-like jacket made of light fabrics. A velcro strip allows attachment of the rat onto a back plate with a rigid bar coming from the robot end-effector. A control interface allows the user to create a virtual environment in which each of the 4 actuated DoFs can be configured independently, from stiff to fully transparent. Typically, we set the X-axis (forward direction) to behave transparently and the Z-axis to provide a constant force proportional to the rat's body weight. The lateral (Y) and rotational (φ) axes were maintained stiff to prevent lateral falls. For specific testing and training, the robot moved the rat's trunk forward at a constant velocity. Consequently, the hindlimbs moved backward and hip joint angle increased towards extension, thus creating conditions that are similar to stepping on a treadmill. Although performed overground, these stepping movements are involuntary. **(C)** Dimension of the horizontal runway. **(D)** Schematic diagrams and features of the different locomotor tasks. The light gray box indicates the position of the force plate for recordings of ground reaction forces (GRF).

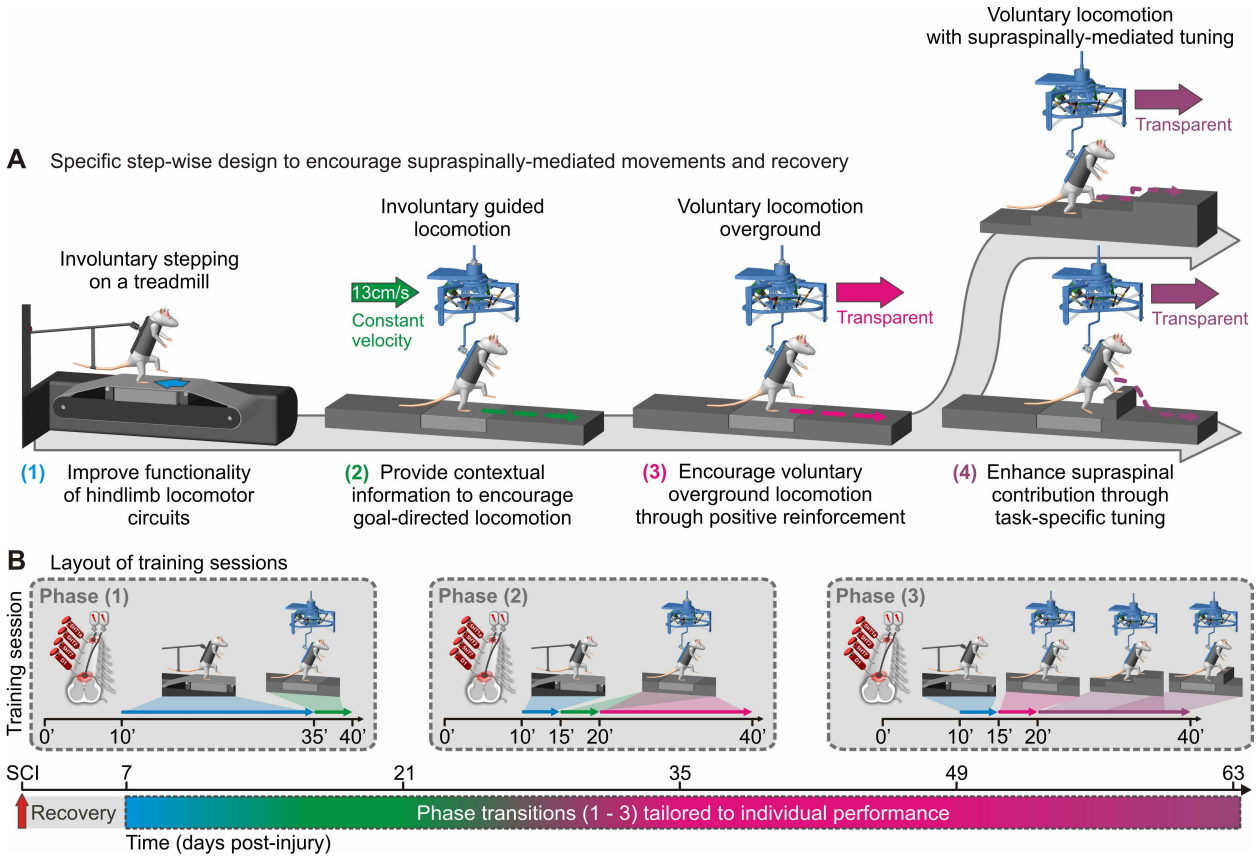

Fig. S3 | Conceptual design of the multi-system neuroprosthetic training program. The **training** consisted of a combination of **(A)** 4 distinct paradigms broadly divided into **(B)** 3 phases specifically tailored to the rats' performance and training objectives. To enable highly functional motor states, rats received monoamine agonists 10 min prior to training, and dual-site EES throughout the session. **Phase (1).** The primary objective of the early training phase was to optimize the functionality of lumbosacral circuits. The rats were subjected to treadmill-based training with vertical support. Sensory input elicited by the moving treadmill belt served as a source of control for hindlimb stepping. Manual assistance was provided in an *assist-as-needed* manner in order to present appropriate sensory cues to lumbosacral circuitries. At the end of each session, we positioned the rats in the robotic postural interface and encouraged them to walk bipedally towards a target located in front of them. The robot was configured to establish optimal medio-lateral and vertical weight support. In order to provide contextual information on the requested task, the robot translated the rat forward at a constant velocity. Positive reinforcement including food rewards and motivational stimuli were used to trigger active participation. The objective was to force the brain to regain supraspinal control over the electrochemically enabled lumbosacral circuits. **Phase (2).** As the rats progressively regained the ability to produce voluntary steps, we gradually increased the duration of locomotion overground. The aim was to encourage the repetitive and quantitative activation of lumbosacral circuits by the newly formed intraspinal and supraspinal connections. However, treadmill-restricted training was still practiced daily in order to engage spinal locomotor circuits over consistent periods of time for the maintenance of their functionality. **Phase (3).** When the rats regained robust hindlimb locomotion overground, we introduced complex tasks requiring fine-tuning of hindlimb movements, i.e. stair climbing and obstacle avoidance. The goal was to promote enhanced supraspinal contribution in order to restore qualitative control over electrochemically enabled lumbosacral circuits.

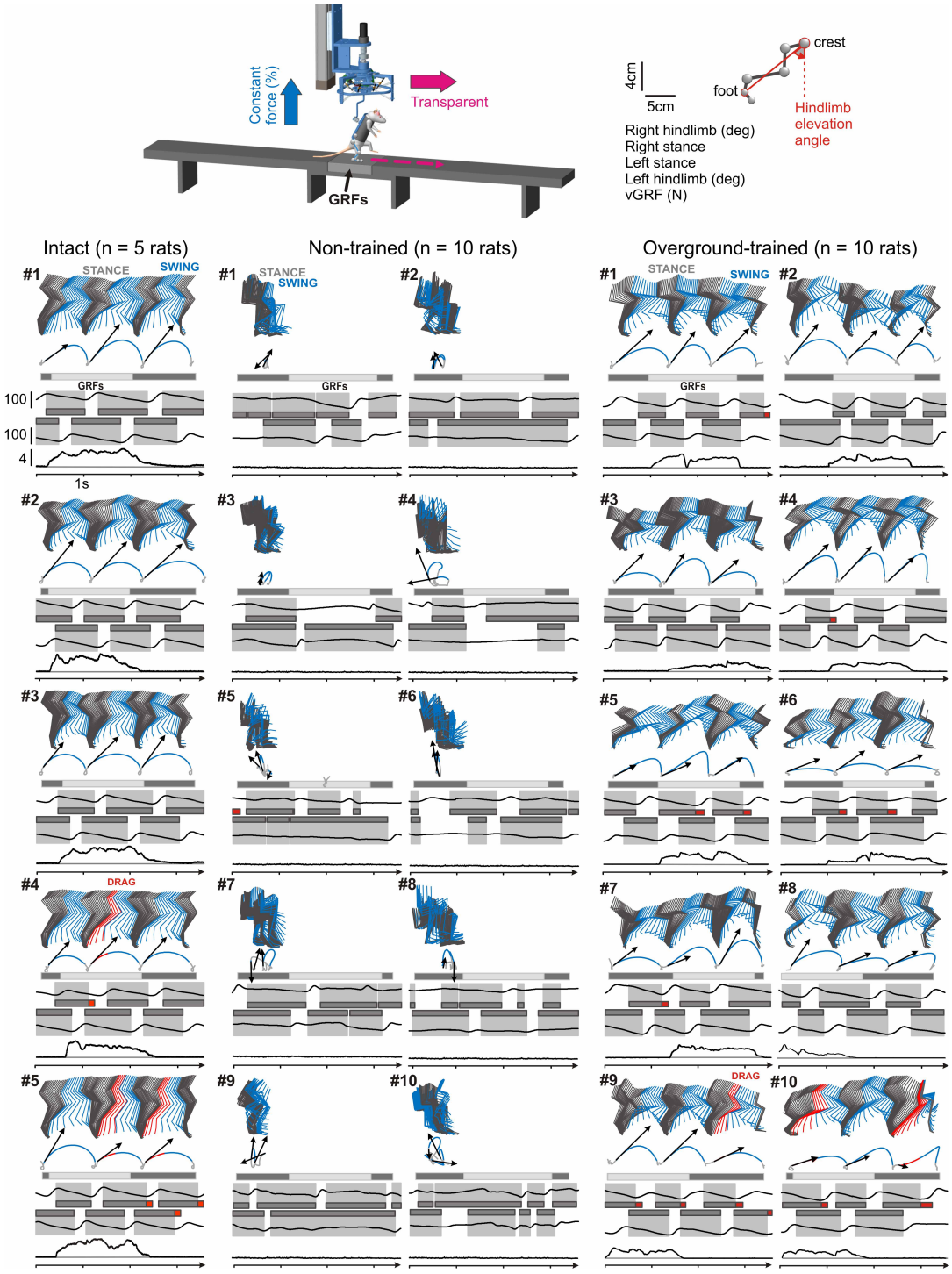

Fig. S4 | Multi-system neuroprosthetic training restores voluntary locomotion overground in all the rats. Representative trials are shown **for five intact animals (left)**, as well as 9 weeks post-injury for each of the non-trained (middle) and overground-trained (right) rats. For each panel, a stick diagram decomposition of hindlimb motion is shown together with color-coded trajectories of the hindlimb endpoint. The hindlimb was defined as the virtual segment connecting the pelvis to the foot. Vectors represent the direction and intensity of the hindlimb endpoint velocity at swing onset. The corresponding sequence of left and right hindlimb oscillations and vertical ground reaction forces (vGRF) are shown below. The light gray rectangle indicates the location of the force plate (GRFs) on the runway. Gray and red bars indicate the duration of stance and drag phases, respectively.

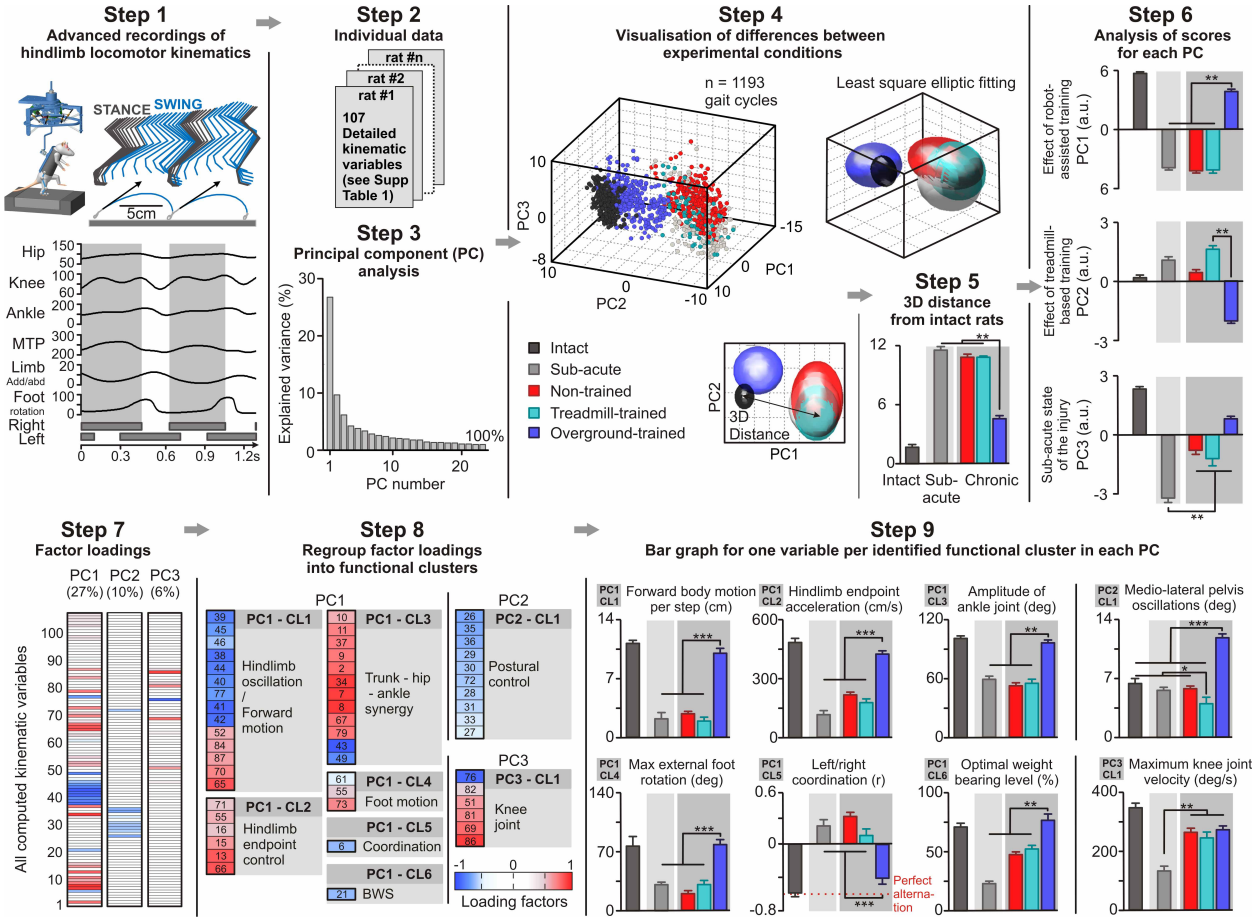

Fig. S5 | Multi-step statistical analysis of locomotor performance and control strategies. Step 1: Advanced recordings of hindlimb kinematics during bipedal overground locomotion. **Step 2:** We computed a large number of variables that provides a holistic quantification of gait. Variables can be found in **Table S1**. **Step 3:** We applied a principal component (PC) analysis on all the variables and recorded gait cycles. **Step 4:** Individual gait cycles can be represented in the new "denoised" space created by PC1-3. We applied a least square elliptic fitting to easily visualise differences between experimental groups. **Step 5:** Locomotor performances were quantified, for each rat, as the 3D Euclidean distance between the location of gait cycles and the average location of all gait cycles from all the intact rats (n = 20 rats). **Step 6:** The scores indicate which experimental groups are differentiated by each PC. **Step 7:** Extraction of factor loadings, i.e. correlation between each gait variable and each PC. **Step 8:** We regrouped variables with the highest factor loading (|value| > 0.5, $p < 0.05$) into functional clusters (CL), which we named for clarity. **Step 9:** To highlight the functional implications of the PC analysis, we generated a histogram plot for one variable per extracted functional cluster. **Conclusions:** PC1 revealed that recovery of voluntary locomotion in overground-trained rats resulted from a strong synergy between ankle extension, trunk extension, and hip flexion, as well as improved interlimb coordination, increased weight bearing capacities, enhanced lateral foot motion, and near-normal control of hindlimb endpoint trajectory. PC2 indicated that treadmill-trained rats showed highly stable posture, but failed to initiate forward locomotion. In turn, overground-trained rats exhibited enhanced lateral body movements that alternatively loaded the left and right hindlimbs during locomotion, and thus helped to maintain dynamic balance. PC3 highlights the flexed posture and slow hindlimb motion of rats in the sub-acute state. a.u., arbitrary unit. **, $P < 0.01$; ***, $P < 0.001$. Error bars, s.e.m.,

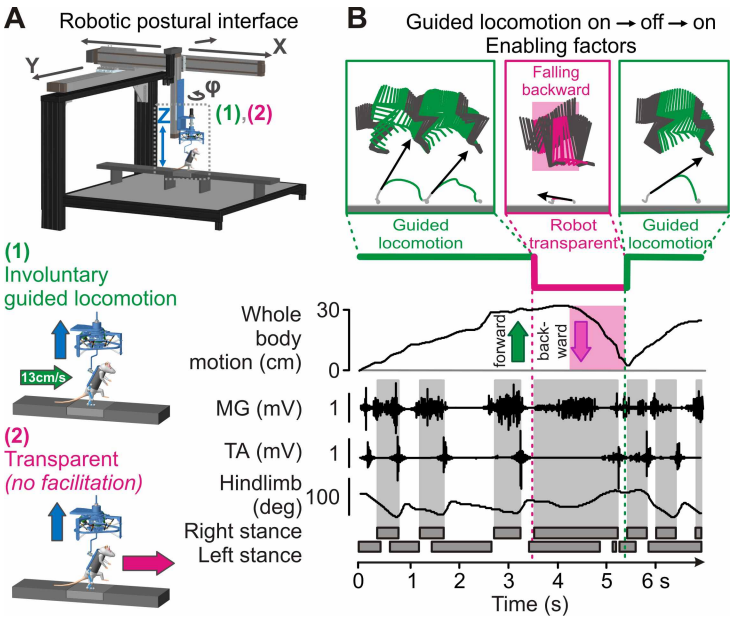

Fig. S6 | Failure to sustain voluntary locomotion overground in treadmill-trained rats. (A) The robotic postural interface can be operated in two modes: **(1)** *involuntary guided locomotion mode* and **(2)** *transparent mode* **(fig. S2)**. **(B)** To test the ability of treadmill-trained rats to sustain voluntary locomotion overground, we programed a sequence during which the robotic postural interface alternated between both modes. Right hindlimb kinematics and EMG activity of right MG and TA muscles are shown according to conventions in **fig. S6** and **Fig. 1**. The position of the whole body along the axis of progression is also represented. When interrupting the robotic guidance, treadmill-trained rats failed to sustain voluntary locomotion overground despite energetic movements with the forelimbs to keep progressing towards a reward, located in front of them. Instead, due to the backward location of the body's center of mass, the rats fell backwards (shaded area). As soon as the robotic guidance was re-applied, the rats displayed coordinated, although involuntary, locomotor movements in the forward direction. These conditions are shown for a representative treadmill-trained rat at 9 weeks post-lesion, but we observed similar behaviors for all the rats in the sub-acute state (1 week post-lesion), as well as for non-trained rats at 9 weeks post-lesion.

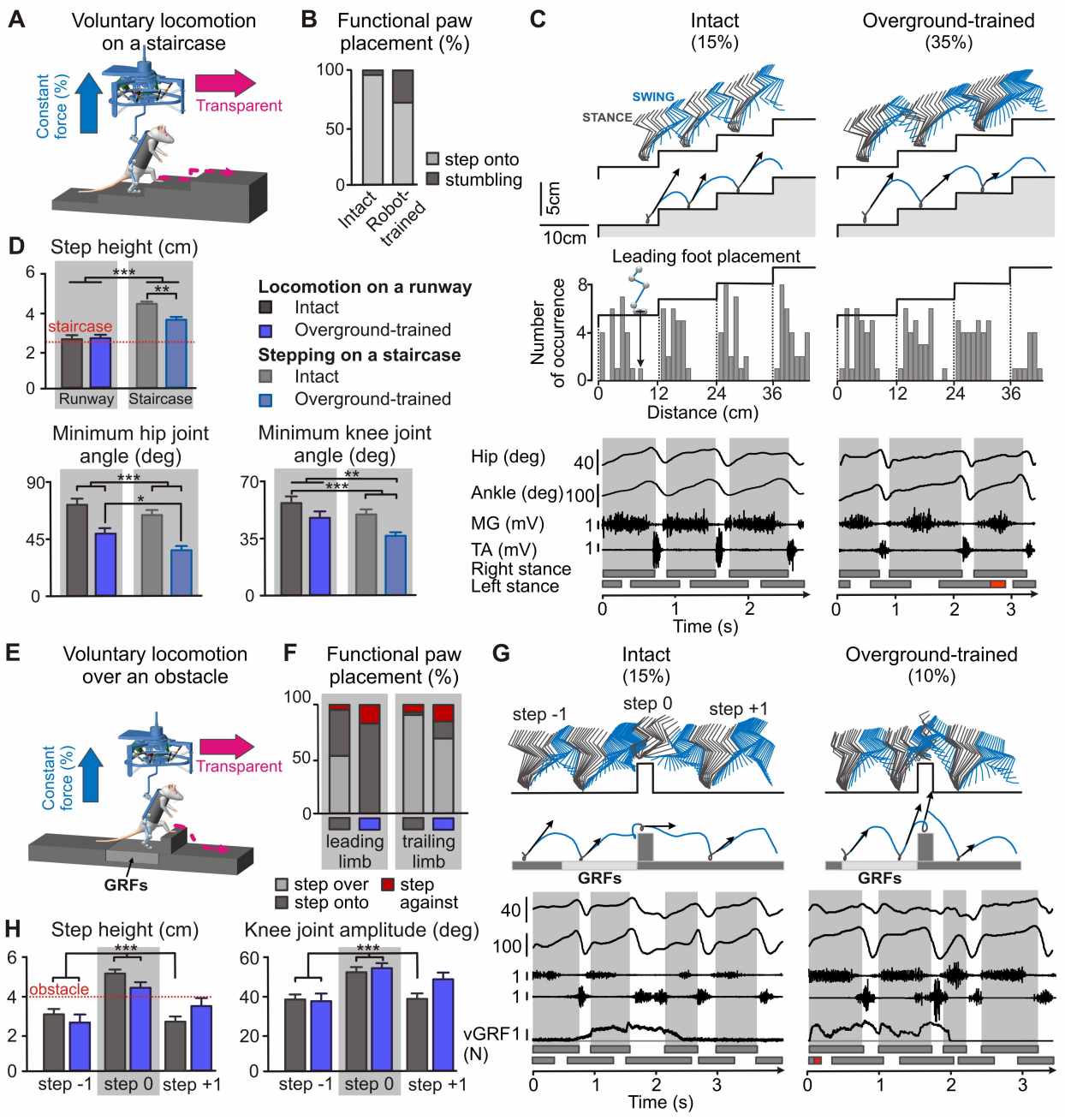

Fig. S7 | Multi-system neuroprosthetic training restores qualitative control of hindlimb locomotor movements. (A) Diagram illustrating bipedal locomotion on a staircase. **(B)** Histograms showing the percentage of correct (step onto) and incorrect (stumbling) hindpaw placements onto each step of the staircase. **(C)** Bipedal locomotion on a staircase for an intact and overground-trained rat. Stick conventions are the same as **Fig. 1** and **fig. S4**. The histogram plots show, for all the intact (n = 5) and overground-trained (n = 10) rats, the distribution of leading foot placements with respect to the positions of the staircases. **(D)** Histogram plots reporting step height as well as the extent of hip and knee flexion during locomotion on a runway and on a staircase for intact and overground-trained rats. **(E)** Diagram illustrating bipedal locomotion over an obstacle. **(F)** Histogram plots showing the percentage of steps performed over and onto the obstacle by the leading and trailing hindlimb for intact and overground-trained rats. **(G)** Bipedal locomotion over an obstacle for an intact and overground-trained rat. **(H)** Histogram plots reporting step height and amplitude changes of the knee joint angle before (step -1), onto (step 0), and after (step +1) the obstacle for intact (n = 5) and overground-trained (n = 10) rats. *, P < 0.05; **, P < 0.01; ***, P < 0.001. Error bars, s.e.m.

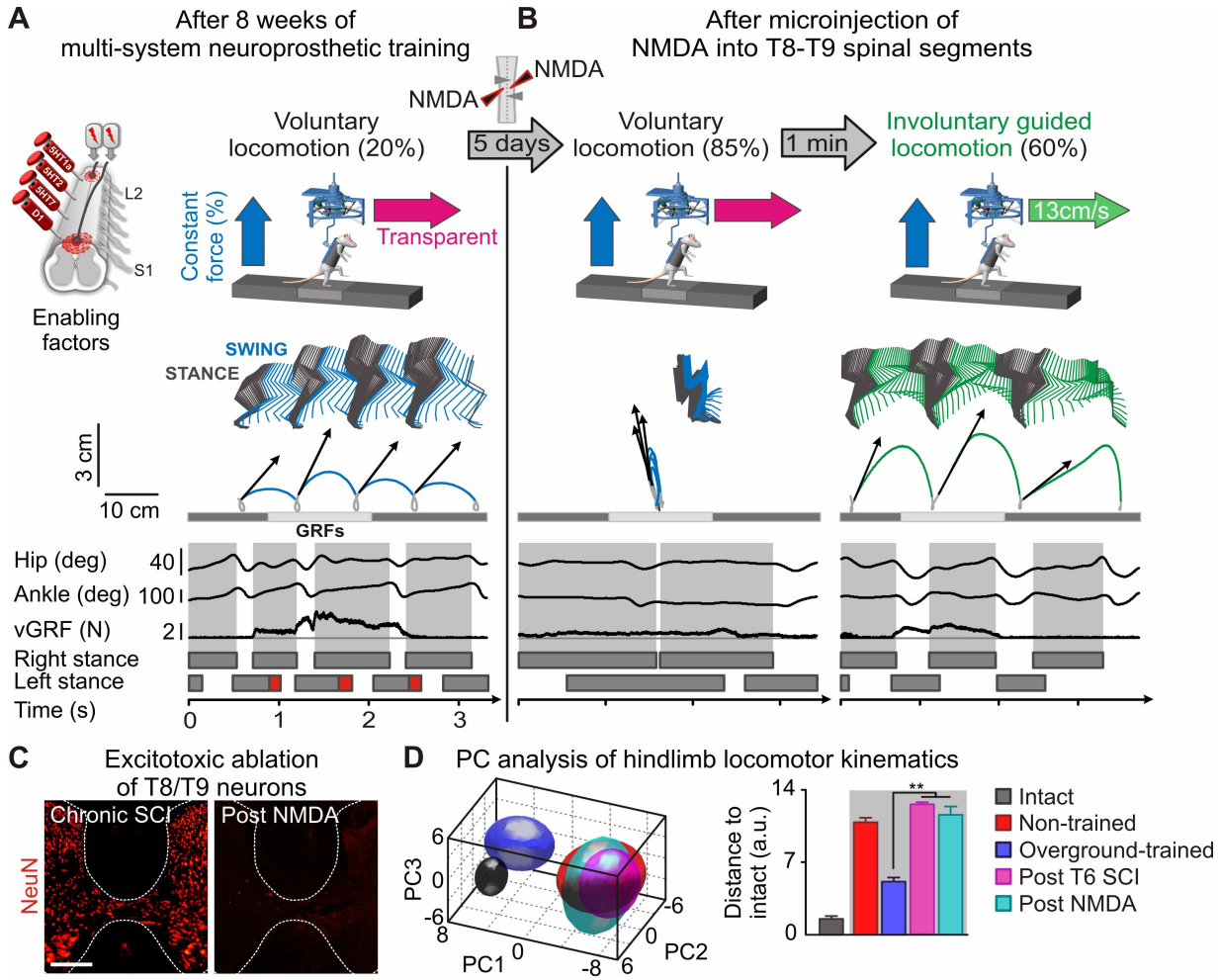

Fig. S8 | Ablation of T8-T9 neurons abolishes voluntary locomotion overground, but leaves spinal locomotor circuitries globally unaffected. Representative example of bipedal locomotion overground in the presence of enabling factors for a overground-trained rat **(A)** before and **(B)** 5 days after microinjections of NMDA into T8-T9 spinal segments. Conventions are the same as in **fig. S4**. The amount of vertical support provided by the robot is indicated in the blue arrow. After NMDA microinjections, the rats failed to initiate voluntary locomotion overground. However, all the tested rats (n = 3) displayed coordinated locomotor movements when the robot moved their body forward at a constant velocity (right panel, 13 cm/s). These results indicate that the loss of thoracic relay neurons interrupted the supraspinal control of locomotion, but did not prevent spinal locomotor circuitries from producing coordinated stepping movements. **(C)** NMDA microinjections ablated the vast majority of neurons in thoracic segments T8-T9. Scale bar, 250µm. **(D)** PC analysis of hindlimb locomotion in intact and non-trained rats, as well as overground-trained rats before the lesion, and after NMDA and complete T6 lesions. The histogram plot reports locomotor performance measured as the distance to intact rats in PC space. **, $P < 0.01$. a.u., arbitrary unit. Error bars, s.e.m.

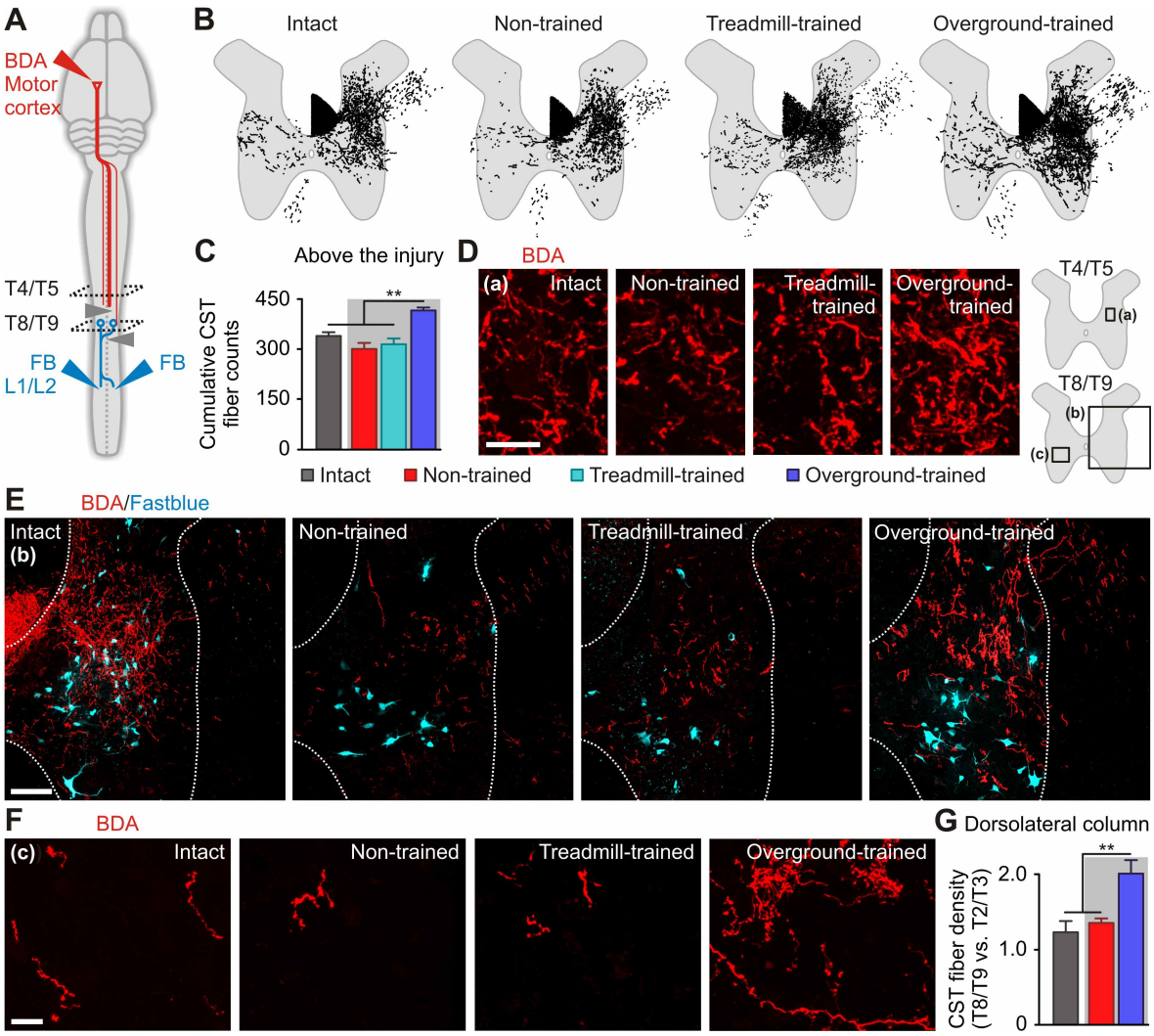

Fig. S9 | Multi-system neuroprosthetic training promotes extensive remodeling of CST projections above and below the SCI. (A) Diagram illustrating anatomical experiments and **analyzed regions**. **(B)** Reconstructions of CST fibers in spinal segments T4-T5, above the injury, for an intact, non-trained, treadmill-trained, and overground-trained rat. **(C)** Bar plots (n = 5 rats per group) and **(D)** confocal images showing density of CST fibers in T4-T5 spinal segments. Scale bar, 20 μm. **(E)** Confocal images showing the density of CST fibers in the right hemicord of T8-T9 spinal segments. Scale bar, 100 μm. **(F)** Confocal images showing the density of CST fibers in the left hemicord of T8-T9 spinal segments. Scale bar, 20 μm. **(G)** Bar plot showing density of CST fibers in the right dorsolateral column (dlCST) at T8/T9 compared to T2/T3 (ratio) (n = 5 rats per group). No differences were found between the experimental groups in the density of dlCST labeling at T2-T3 ($p = 0.53$). **, $P < 0.01$. Error bars, s.e.m.

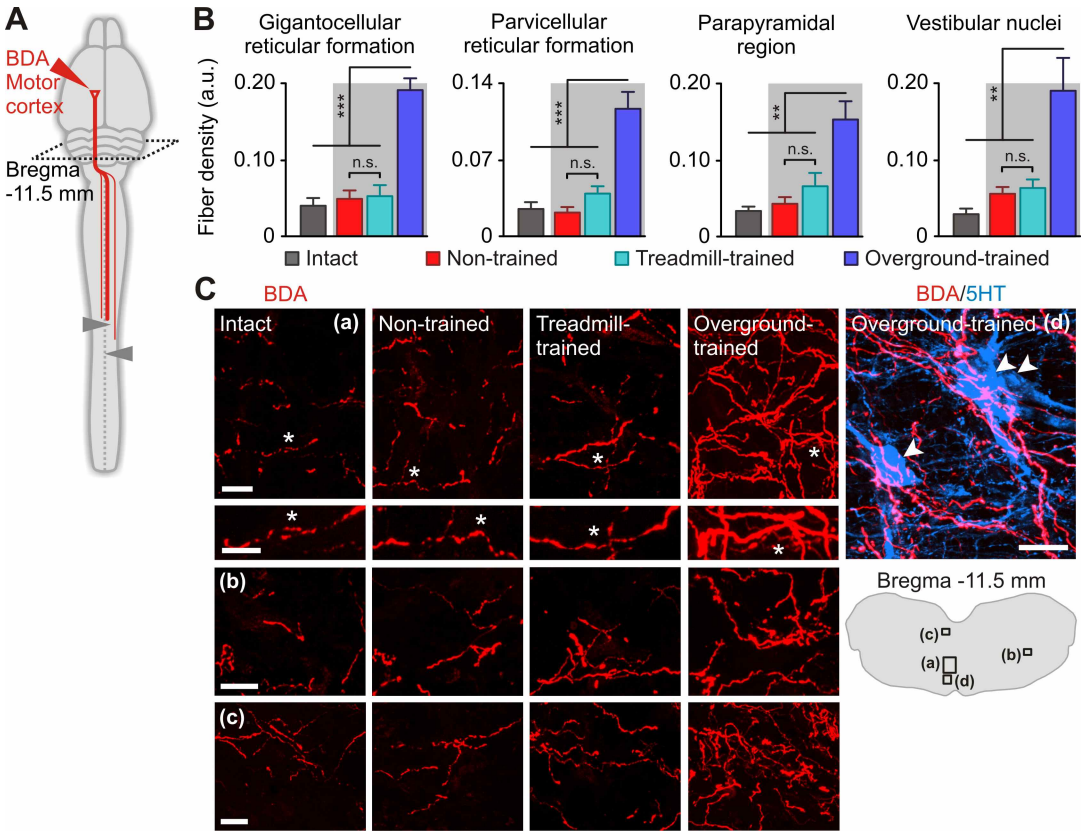

Fig. S10 | Multi-system neuroprosthetic training promotes extensive remodeling of motor cortex axonal projections in brainstem locomotor regions. (A) Diagram illustrating anatomical experiments **and analyzed regions**. **(B)** Bar plots (n = 5 rats per group) reporting the density of motor cortex originating fibers in the gigantocellular reticular formation, parvicellular reticular formation, parapyramidal region, and vestibular nuclei for intact, non-trained, treadmill-trained and overground-trained rats. **(C)** Representative confocal images showing the density of motor cortex originating fibers in the various brainstem locomotor regions (a) – (c). We detected unusually dense motor cortex axonal projections in the vicinity of locomotor-related serotonergic (5HT) neurons (arrows) in overground-trained rats (d). Scale bar, 20 µm. **, $P < 0.01$; ***, $P < 0.001$. n.s., non significant; a.u., arbitrary unit. Error bars, s.e.m.,

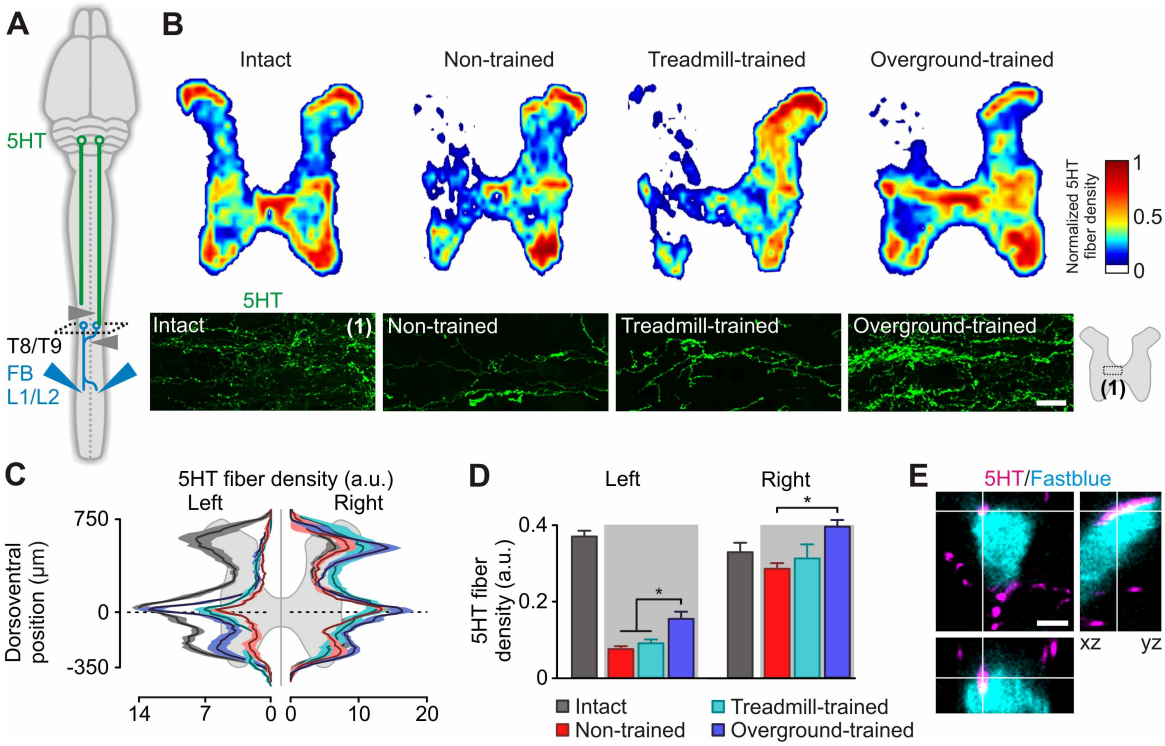

Fig. S11 | Multi-system neuroprosthetic training promotes extensive remodeling of brainstem-derived serotonergic projections. **(A)** Diagram illustrating anatomical experiments including the source of spinal 5HT projections in the brainstem. **(B)** Heat maps showing 5HT fiber density in T8-T9 segments and confocal images showing midline crossing 5HT fibers in intermediate laminae, close to the central canal. Scale bar, 20µm. **(C)** Distribution of 5HT fiber density along the dorsoventral extent of T8-T9 segments. **(D)** Bar graphs reporting 5HT fiber density in the left and right T8-T9 hemicords. **(D)** Confocal images showing close appositions between 5HT fibers and a thoracic relay neuron retrogradely labeled from L1-L2 locomotor centers in a overground-trained animal. Scale bar, 5µm. a.u., arbitrary unit. *, $P < 0.05$. Error bars, s.e.m.

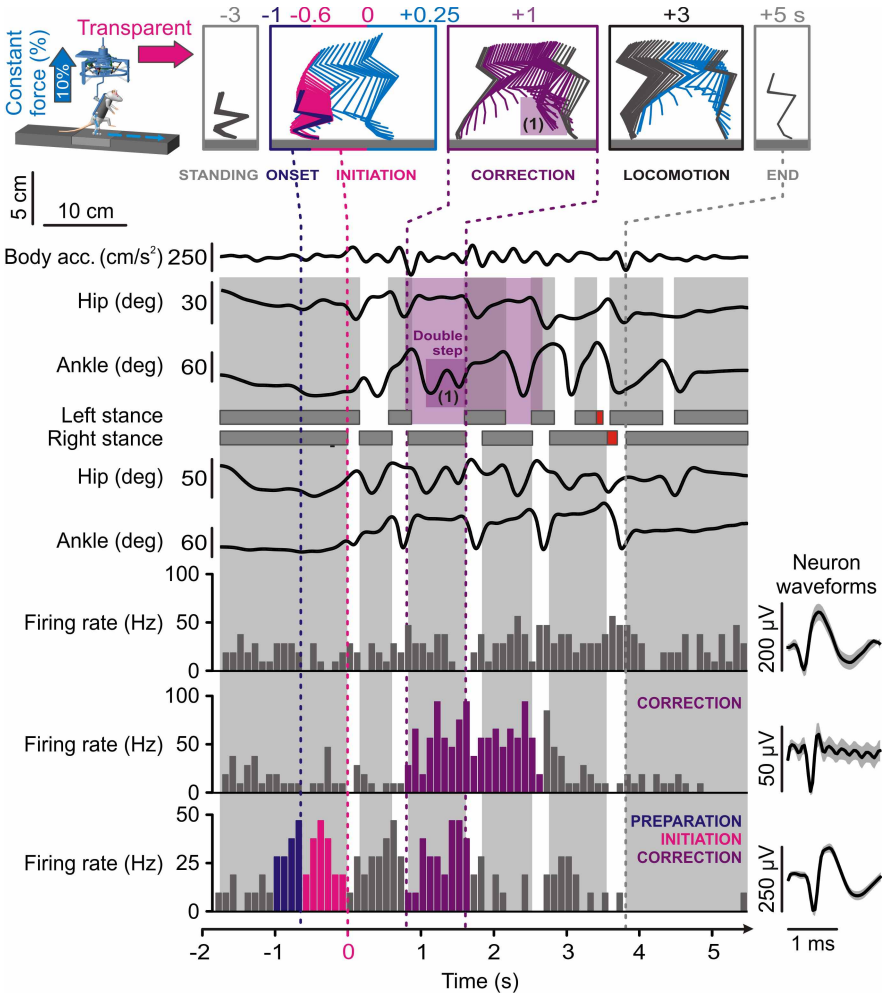

Fig. S12 | Left motor cortex neuronal modulations correlate with gait initiation and correction. A representative sequence including gait initiation and correction of locomotor movement is shown for a overground-trained rat. Stick diagram decompositions of hindlimb motion are displayed to highlight the various gait events. The corresponding changes in body acceleration (acc.), left and right hindlimb joint angles, and neuronal firing rates of 3 motor cortex neurons are shown below together with the duration of stance (gray), swing (empty), and drag (red). Neuron waveforms are displayed as means +/- S.D. Neuronal firing rates were estimated in 100 ms windows, and color-coded according to the period during which significant changes were found. Significance was tested by comparing the distributions of firing rates relative to *initiation* or *correction* events. If there was a significant change in firing rate within any successive pair of one-second windows from 2 s before to 1 s after the event, the neuron was classified as significantly modulated. *Initiation* was defined as the initial foot clearance. *Preparation* corresponded to the period during which a significant increase in firing rate was detected relative to standing, but no overt gait-related movement (onset, hip extension) had yet taken place. *Correction* included a sequence of three events: a step resulting in negative body acceleration superior to 80 cm/s^2, a subsequent contralateral double-step without paw placement (1), and an ipsilateral step/hop before the contralateral paw had been fully placed. The foot clearance of the third event in this sequence was defined as the time of correction. The first neuron showed no significant modulation with respect to *initiation* or *correction*. The second neuron displayed a significant increase in firing rate 1 s before and after the *correction* event. The third neuron exhibited significant changes in firing rates 1 s before *initiation* and 1 s before *correction*.

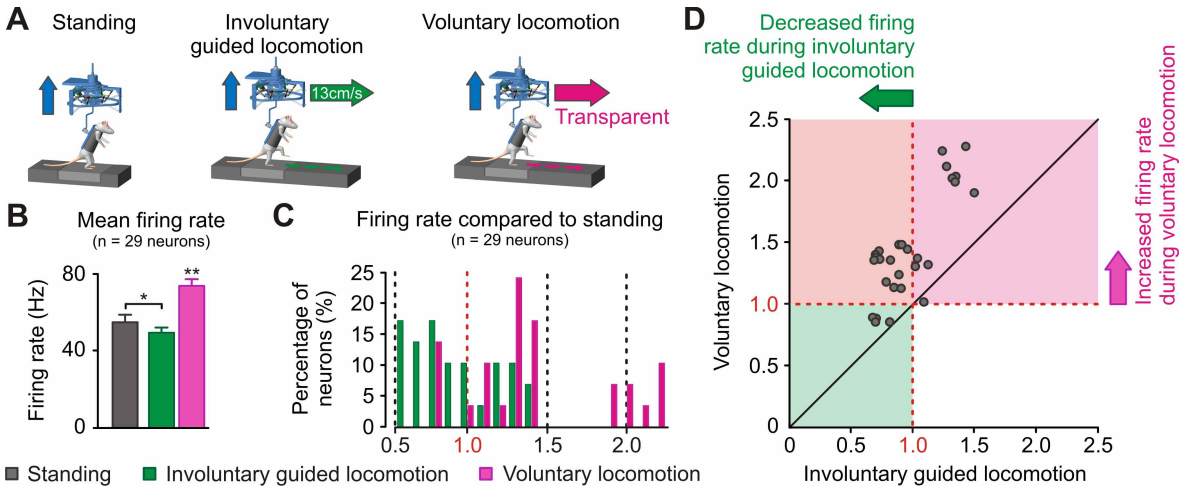

Fig. S13 | Left motor cortex neurons showed decreased firing rate during involuntary guided locomotion. (A) Neuronal modulations were recorded during standing, involuntary guided locomotion, and voluntary locomotion. **(B)** Bar graphs reporting average values (n = 29 neurons) of mean firing rate for each experimental condition. **(C)** Distribution of mean firing rate normalized to standing for all the recorded neurons. **(D)** Mean firing rate during involuntary guided locomotion is plotted against mean firing rate during voluntary locomotion. The majority of neurons that showed increased firing rate during voluntary locomotion exhibited a significant ($p < 0.05$) decrease in firing rate during involuntary guided locomotion (red). A cluster of neurons displayed increased firing rates during both paradigms, but the extent of the modulation was more pronounced during voluntary than involuntary locomotion (magenta). *, $P < 0.05$; **, $P < 0.01$. Error bars, s.e.m.

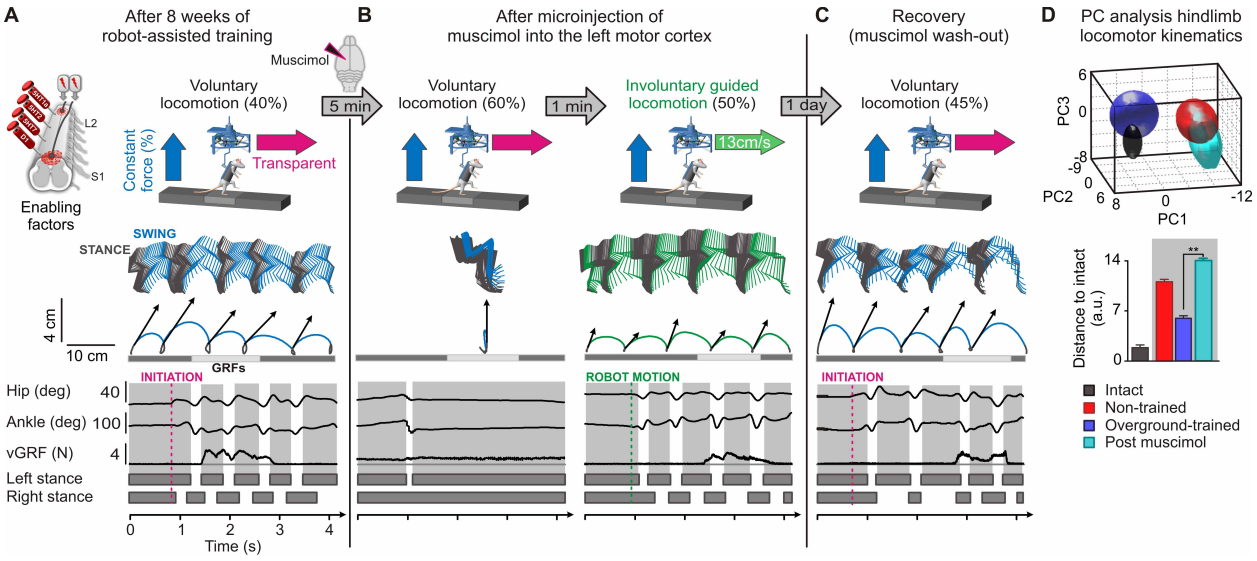

Fig. S14 | Microinjections of muscimol into the motor cortex abolish voluntary locomotion overground, but leave spinal locomotor circuitries globally unaffected. Representative example of bipedal locomotion overground in the presence of enabling factors for a overground-trained rat **(A)** before and **(B)** 5 min after a microinjection of muscimol into the left motor cortex. Hindlimb locomotor kinematics and vGRFs are shown using the same conventions as in **fig. S4**. The amount of vertical support provided by the robot is indicated above each panel (%). Muscimol microinjections immediately abolished voluntary locomotion overground. However, all the tested rats (n = 3) displayed coordinated locomotor movements during involuntary guided locomotion (13 cm/s). These results indicate that the inactivation of the motor cortex suppressed the ability to initiate voluntary locomotion, but did not prevent spinal locomotor circuitries from producing coordinated stepping movements. **(C)** One day after muscimol microinjection, the rats recovered voluntary locomotion overground. **(D)** PC analysis of hindlimb locomotion in intact and non-trained rats, as well as overground-trained rats before and after muscimol microinjection. The histogram plot reports locomotor performance measured as the distance to intact rats in PC space. **, $P < 0.01$. a.u., arbitrary unit. Error bars, s.e.m

Table S1. Computed kinematics and gait parameters for principal component (PC) analysis

Parameters		#	Detailed explanation
Kinematics			
Temporal features of gait			
		1	Cycle duration
		2	Cycle velocity
		3	Stance duration
		4	Stance duration (%)
		5	Relative stance duration (percent of the cycle duration)
		6	Interlimb coordination (cross-correlation between hindlimbs)
Limb endpoint (MTP) trajectory			
		7	Stride length
		8	Step length
		9	3D limb endpoint path length
		10	Maximum backward position
		11	Minimum forward position
		12	Step height
		13	Maximum speed during swing
		14	Relative timing of maximum velocity during swing
		15	Acceleration at swing onset
		16	Endpoint velocity
		17	Orientation of the velocity vector at swing onset
		18	Dragging
		19	Relative dragging duration (percent of swing duration)
Stability			
Base of support		20	Positioning of the foot at stance onset with respect to the pelvis
		21	Amount of robotic vertical support (%)
Trunk and pelvic position and oscillations		22	Stance width
		23	Maximum trunk vertical position
		24	Minimal trunk vertical position
		25	Amplitude of trunk vertical movement
		26	Variability of sagittal trunk oscillations
		27	Variability in velocity of sagittal trunk oscillations
		28	Variability of Medio-lateral hip oscillations
		29	Variability of vertical mid-point hip oscillations
		30	Variability of Medio-lateral mid-point shoulder oscillations
		31	Variability of vertical mid-point shoulder oscillations
		32	Variability of Medio-lateral shoulder rotations
		33	Variability of Medio-lateral hip rotations
Whole Body movement			
Displacement of the body mid-point (pelvis)		34	Forward motion
		35	Medio-lateral motion
		36	Vertical motion
		37	3D motion
Joint angles and segmental oscillations			
Backward	proximal	38	Crest oscillations
		39	Thigh oscillations
		40	Leg oscillations
		41	Foot oscillations
	distal	42	Toe oscillations
	whole limb	43	Whole limb oscillations
Forward	proximal	44	Crest oscillations
		45	Thigh oscillations
		46	Leg oscillations
		47	Foot oscillations
	distal	48	Toe oscillations
	whole limb	49	Whole limb oscillations
Flexion	proximal	50	Hip joint angle
		51	Knee joint angle
		52	Ankle joint angle
	distal	53	MTP joint angle

Parameters		#	Detailed explanation
Kinematics			
Joint angles and segmental oscillations			
Abduction	whole limb	54	Whole limb abduction
	distal	55	Foot abduction
Extension	proximal	56	Hip joint angle
		57	Knee joint angle
		58	Ankle joint angle
	distal	59	MTP joint angle
Adduction	whole limb	60	Whole limb adduction
	distal	61	Foot adduction
Amplitude	proximal	62	Crest oscillations
		63	Thigh oscillations
		64	Leg oscillations
		65	Foot oscillations
	distal	66	Toe oscillations
	whole limb	67	Whole limb oscillations
	proximal	68	Hip joint angle
		69	Knee joint angle
		70	Ankle joint angle
	distal	71	MTP joint angle
	whole limb	72	Whole limb medio-lateral oscillations
	distal	73	Foot abduction /adduction
Velocity			
Minimum	whole limb	74	Whole limb oscillation velocity
	proximal	75	Hip joint angle velocity
		76	Knee joint angle velocity
		77	Ankle joint angle velocity
	distal	78	MTP joint angle velocity
Maximum	whole limb	79	Whole limb oscillation velocity
	proximal	80	Hip joint angle velocity
		81	Knee joint angle velocity
		82	Ankle joint angle velocity
	distal	83	MTP joint angle velocity
Amplitude	whole limb	84	Whole limb angle velocity
	proximal	85	Hip joint angle velocity
		86	Knee joint angle velocity
		87	Ankle joint angle velocity
	distal	88	MTP joint angle velocity
Inter-limb coordination			
PC analysis		89	Degree of linearity in bilateral hindlimb coordination (PC analysis)
		90	Degree of linear coupling in intralimb coordination (PC analysis)
		91	Degree of linear coupling in intralimb coordination (PC analysis)
FFT decomposition	proximal	92	Temporal coupling between crest and thigh oscillations
		93	Temporal coupling between thigh and leg oscillations
		94	Temporal coupling between leg and foot oscillations
	distal	95	Temporal coupling between foot and toe oscillations
Cross-correlation	proximal	96	Correlation between crest and tight oscillations
		97	Correlation between tight and leg oscillations
		98	Correlation between leg and foot oscillations
		99	Correlation between foot and toe oscillations
		100	Correlation between hip and knee oscillations
		101	Correlation between knee and ankle oscillations
	distal	102	Correlation between ankle and MTP oscillations
Similarity to intact rats			
Cross-correlation between intact and lesioned	whole limb	103	Hindlimb
	proximal	104	Hip
		105	Knee
		106	Ankle
	distal	107	MTP

Table S1 | Computed kinematics and gait parameters for principal component (PC) analysis.

References

1. H. Barbeau, S. Rossignol, Recovery of locomotion after chronic spinalization in the adult cat. *Brain Res.* **412**, 84 (1987).

2. R. G. Lovely, R. J. Gregor, R. R. Roy, V. R. Edgerton, Effects of training on the recovery of full-weight-bearing stepping in the adult spinal cat. *Exp. Neurol.* **92**, 421 (1986).

3. A. Wernig, S. Müller, Laufband locomotion with body weight support improved walking in persons with severe spinal cord injuries. *Paraplegia* **30**, 229 (1992).

4. A. Wernig, S. Müller, A. Nanassy, E. Cagol, Laufband therapy based on 'rules of spinal locomotion' is effective in spinal cord injured persons. *Eur. J. Neurosci.* **7**, 823 (1995).

5. S. Harkema *et al*., Effect of epidural stimulation of the lumbosacral spinal cord on voluntary movement, standing, and assisted stepping after motor complete paraplegia: A case study. *Lancet* **377**, 1938 (2011).

6. G. Courtine *et al*., Transformation of nonfunctional spinal circuits into functional states after the loss of brain input. *Nat. Neurosci.* **12**, 1333 (2009).

7. B. A. Kakulas, A review of the neuropathology of human spinal cord injury with emphasis on special features. *J. Spinal Cord Med.* **22**, 119 (1999).

8. G. Courtine *et al*., Recovery of supraspinal control of stepping via indirect propriospinal relay connections after spinal cord injury. *Nat. Med.* **14**, 69 (2008).

9. P. Musienko, J. Heutschi, L. Friedli, R. V. den Brand, G. Courtine, Multi-system neurorehabilitative strategies to restore motor functions following severe spinal cord injury. *Exp. Neurol.* **235**, 100 (2012).

10. P. Musienko *et al*., Controlling specific locomotor behaviors through multidimensional monoaminergic modulation of spinal circuitries. *J. Neurosci.* **31**, 9264 (2011).

11. G. H. Guyatt *et al*., The 6-minute walk: A new measure of exercise capacity in patients with chronic heart failure. *Can. Med. Assoc. J.* **132**, 919 (1985).

12. T. Drew, J. E. Andujar, K. Lajoie, S. Yakovenko, Cortical mechanisms involved in visuomotor coordination during precision walking. *Brain Res. Brain Res. Rev.* **57**, 199 (2008).

13. F. M. Bareyre *et al*., The injured spinal cord spontaneously forms a new intraspinal circuit in adult rats. *Nat. Neurosci.* **7**, 269 (2004).

14. K. C. Cowley, E. Zaporozhets, B. J. Schmidt, Propriospinal neurons are sufficient for bulbospinal transmission of the locomotor command signal in the neonatal rat spinal cord. *J. Physiol.* **586**, 1623 (2008).

15. C. Brösamle, M. E. Schwab, Cells of origin, course, and termination patterns of the ventral, uncrossed component of the mature rat corticospinal tract. *J. Comp. Neurol.* **386**, 293 (1997).

16. E. S. Rosenzweig *et al*., Extensive spontaneous plasticity of corticospinal projections after primate spinal cord injury. *Nat. Neurosci.* **13**, 1505 (2010).

17. O. Steward, B. Zheng, M. Tessier-Lavigne, False resurrections: Distinguishing regenerated from spared axons in the injured central nervous system. *J. Comp. Neurol.* **459**, 1 (2003).

18. M. Hägglund, L. Borgius, K. J. Dougherty, O. Kiehn, Activation of groups of excitatory neurons in the mammalian spinal cord or hindbrain evokes locomotion. *Nat. Neurosci.* **13**, 246 (2010).

19. J. Liu, L. M. Jordan, Stimulation of the parapyramidal region of the neonatal rat brain stem produces locomotor-like activity involving spinal 5-HT7 and 5-HT2A receptors. *J. Neurophysiol.* **94**, 1392 (2005).

20. G. Courtine *et al*., Can experiments in nonhuman primates expedite the translation of treatments for spinal cord injury in humans? *Nat. Med.* **13**, 561 (2007).

21. L. T. Alto *et al*., Chemotropic guidance facilitates axonal regeneration and synapse formation after spinal cord injury. *Nat. Neurosci.* **12**, 1106 (2009).

22. F. Sun *et al*., Sustained axon regeneration induced by co-deletion of PTEN and SOCS3. *Nature* **480**, 372 (2011).

23. V. R. Edgerton *et al*., Training locomotor networks. *Brain Res. Brain Res. Rev.* **57**, 241 (2008).

24. L. L. Cai *et al*., Implications of assist-as-needed robotic step training after a complete spinal cord injury on intrinsic strategies of motor learning. *J. Neurosci.* **26**, 10564 (2006).

25. A. Wernig, "Ineffectiveness" of automated locomotor training. *Arch. Phys. Med. Rehabil.* **86**, 2385 (2005).

26. M. Wirz *et al*., Effectiveness of automated locomotor training in patients with chronic incomplete spinal cord injury: A multicenter trial. *Arch. Phys. Med. Rehabil.* **86**, 672 (2005).

27. P. Musienko, R. van den Brand, O. Maerzendorfer, A. Larmagnac, G. Courtine, Combinatory electrical and pharmacological neuroprosthetic interfaces to regain motor function after spinal cord injury. *IEEE Trans. Biomed. Eng.* **56**, 2707 (2009).

28. R. Fuentes, P. Petersson, W. B. Siesser, M. G. Caron, M. A. Nicolelis, Spinal cord stimulation restores locomotion in animal models of Parkinson's disease. *Science* **323**, 1578 (2009).

29. S. Micera, A. M. Sabatini, P. Dario, B. Rossi, A hybrid approach to EMG pattern analysis for classification of arm movements using statistical and fuzzy techniques. *Med. Eng. Phys.* **21**, 303 (1999).

30. R. Q. Quiroga, Z. Nadasdy, Y. Ben-Shaul, Unsupervised spike detection and sorting with wavelets and superparamagnetic clustering. *Neural Comput.* **16**, 1661 (2004).

31. M. S. Lewicki, A review of methods for spike sorting: The detection and classification of neural action potentials. *Network* **9**, R53 (1998).

32. J. B. Carmel, L. J. Berrol, M. Brus-Ramer, J. H. Martin, Chronic electrical stimulation of the intact corticospinal system after unilateral injury restores skilled locomotor control and promotes spinal axon outgrowth. *J. Neurosci.* **30**, 10918 (2010).